Supporting Information

Unravelling the Active Vanadium Sites and Adsorbate Dynamics in VO_x/CeO_2 Oxidation Catalysts Using Transient IR Spectroscopy

Leon Schumacher, Jakob Weyel, Christian Hess*

Eduard Zintl Institute for Inorganic and Physical Chemistry, Technical University of Darmstadt, Alarich-Weiss-Str. 8, 64287 Darmstadt, Germany

*Corresponding Author (E-Mail: christian.hess@tu-darmstadt.de)

Table of Contents:

1) Technical Information

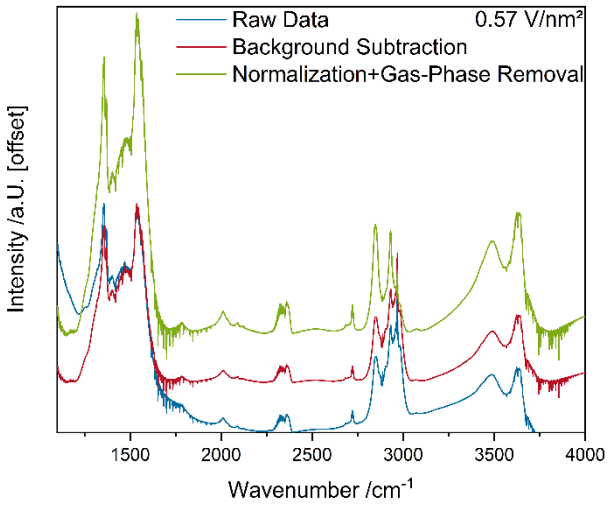

Figure S1: Representation of data processing of the DRIFT spectra, shown for the 0.57 V/nm² sample as an example. For details, please refer to the experimental section.

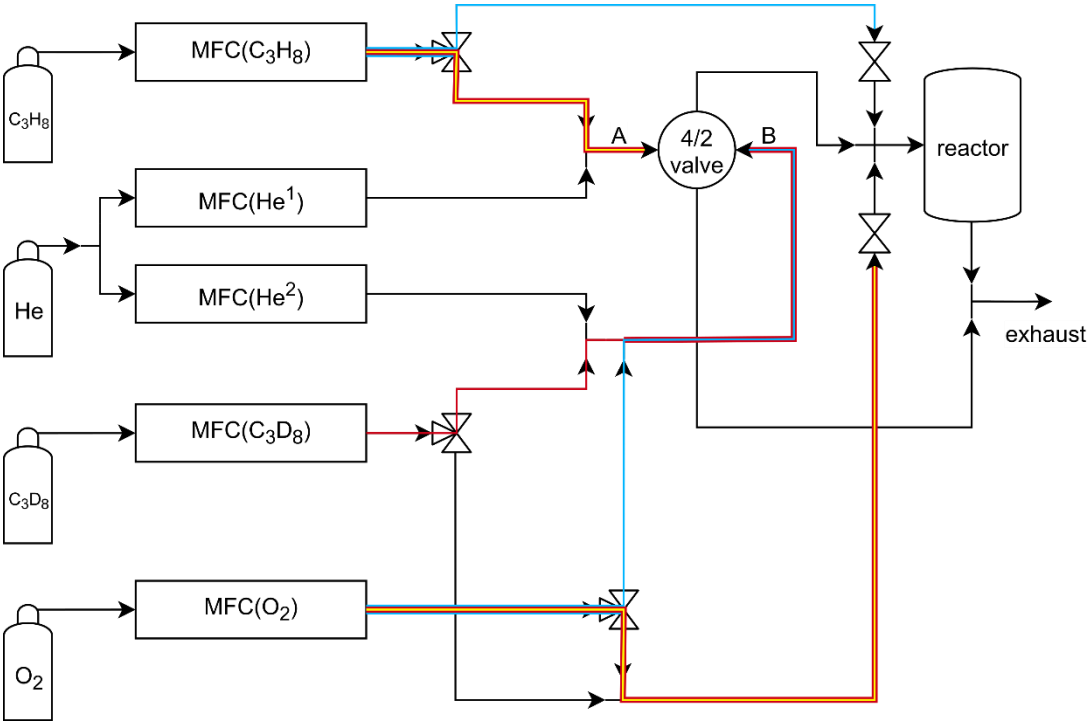

Figure S2: Experimental setup used for ME-DRIFTS. The different gas feeds for the three types of modulation experiments are highlighted in different colors. Orange: constant oxygen flow, pulsed propane flow. Blue: constant propane flow, pulsed oxygen flow. Red: constant oxygen flow, alternating flows of propane and propane-d8.

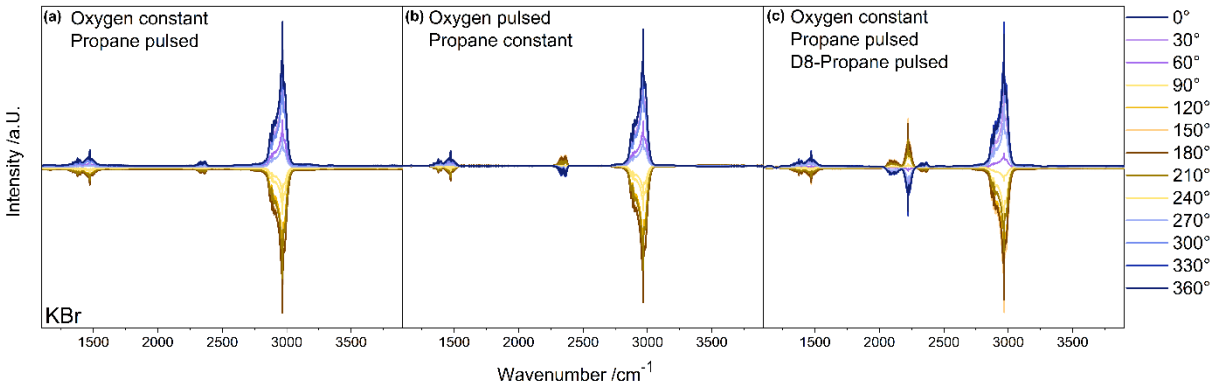

Figure S3: KBr spectra recorded in different gas-phase environments, used as background in ME-DRIFTS experiments. **a**: constant oxygen flow, pulsed propane flow; **b**: constant propane flow, pulsed oxygen flow; **c**: constant oxygen flow, pulsed propane-h_8/-d_8 flow.

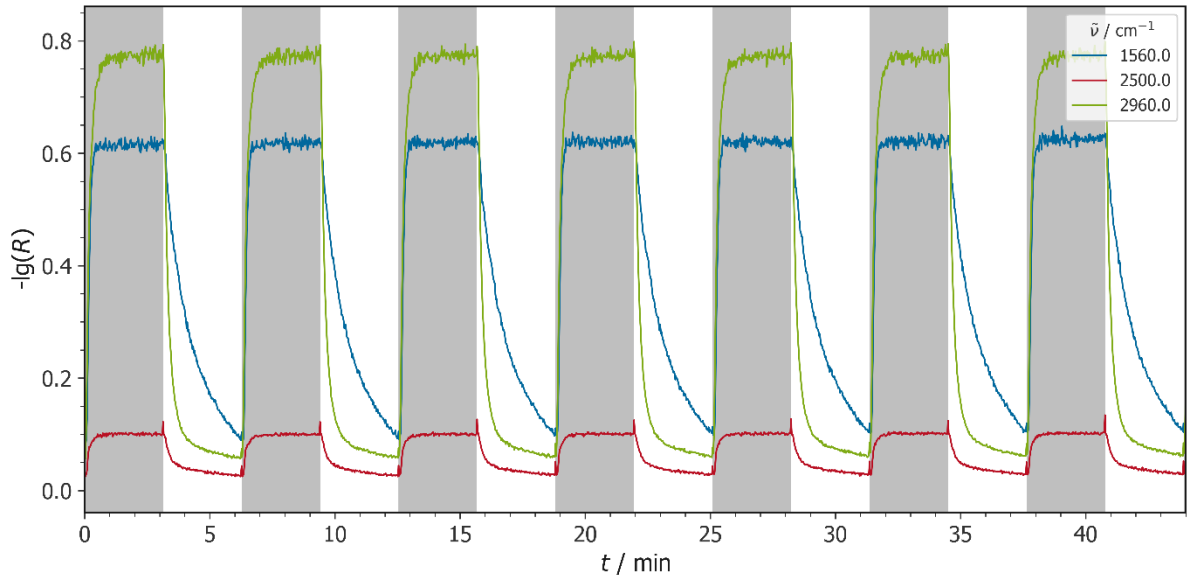

Figure S4: ME-DRIFTS course plot for the 0.57 V/nm² sample at 1560 cm^{-1}, 2500 cm^{-1}, and 2960 cm^{-1}. These wavenumbers were chosen to represent the position of an adsorbate peak, the background, and a propane gas-phase peak, respectively.

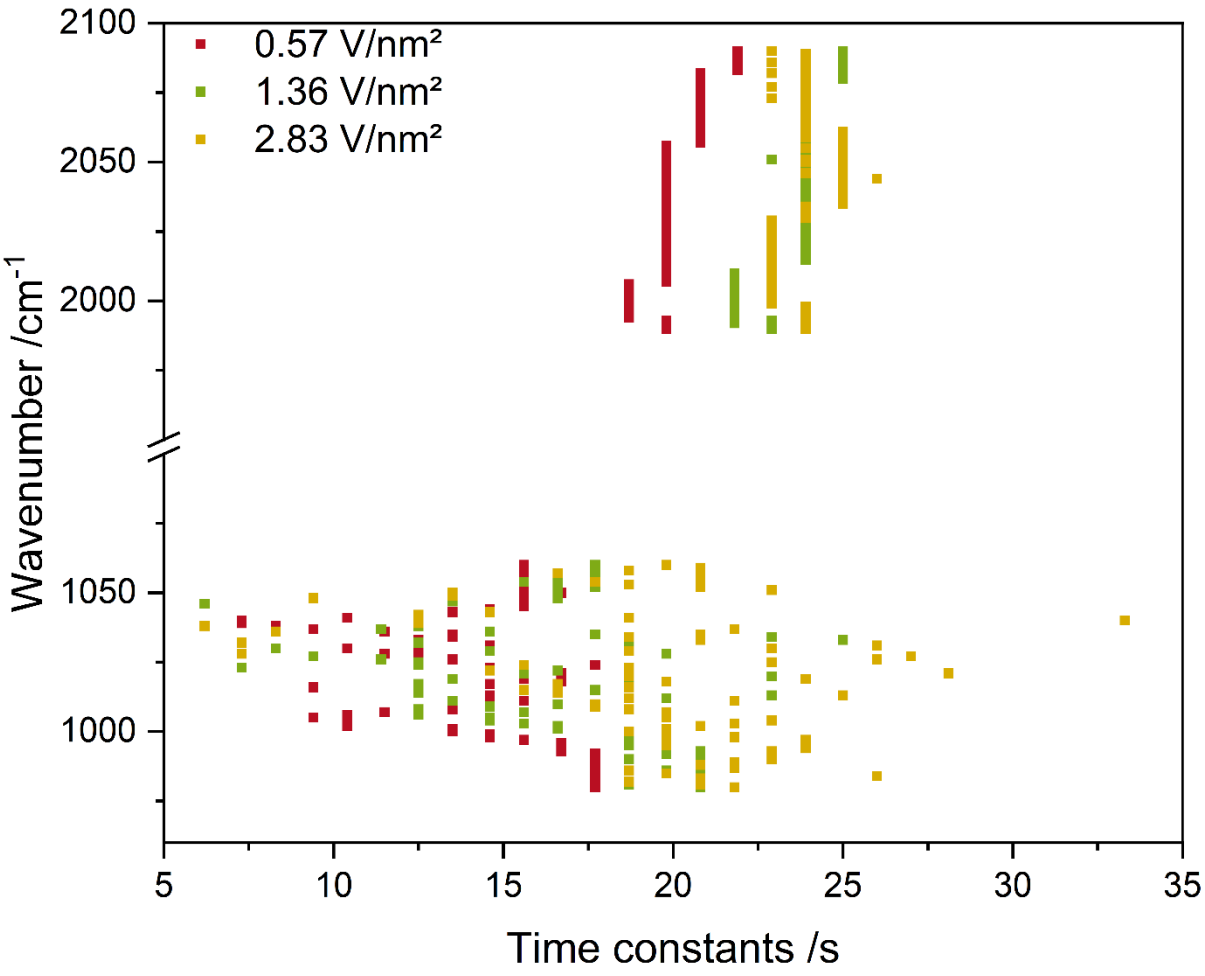

Figure S5: Time constants from the in-phase angle analysis of the vanadyl fundamental (980–1060 cm^{-1}) and overtone region (1990–2090 cm^{-1}) with a resolution of 1 cm^{-1}.

Figure S5 reveals that the time constants in the vanadyl fundamental region (980–1060 cm^{-1}) show a wide variation between 7 and 34 s, whereas those in the overtone region are much more condensed. Since there is no physical reason why the fundamental and overtone vibrations should show different time constants (significantly outside the margin of error), we attribute this behavior to an overlap of the vanadyl fundamental region with a broad Ce-O peak from either a Ce-OH group[1,2] or a carbonate[3] that is permanently present on the catalyst surface. The ceria peak is observable in the regular DRIFT spectra as well as the ME-DRIFT spectra between 1020 and 1080 cm^{-1} (compare Figs. 1c, S16, and S17). The variation of the vanadyl fundamental vibration is proposed to be caused by the Ce-O or O-C-O vibration in the same region. Therefore, the time constants of the overtone were used for the mechanistic evaluation.

2) Characterization Data, Selectivities and Temperature-Dependent DRIFTS

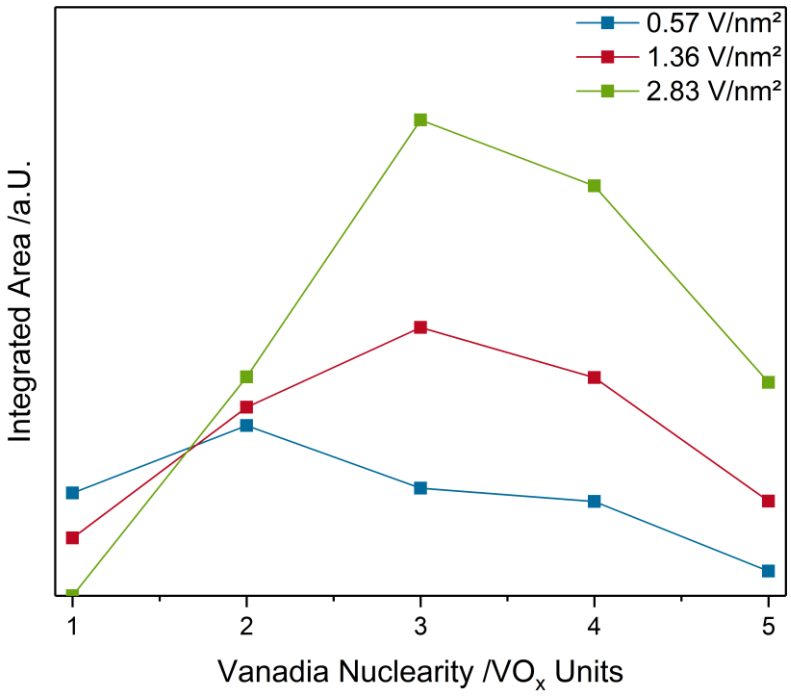

Figure S6: Loading-dependent nuclearity distribution of vanadia species based on 514 nm Raman spectra.

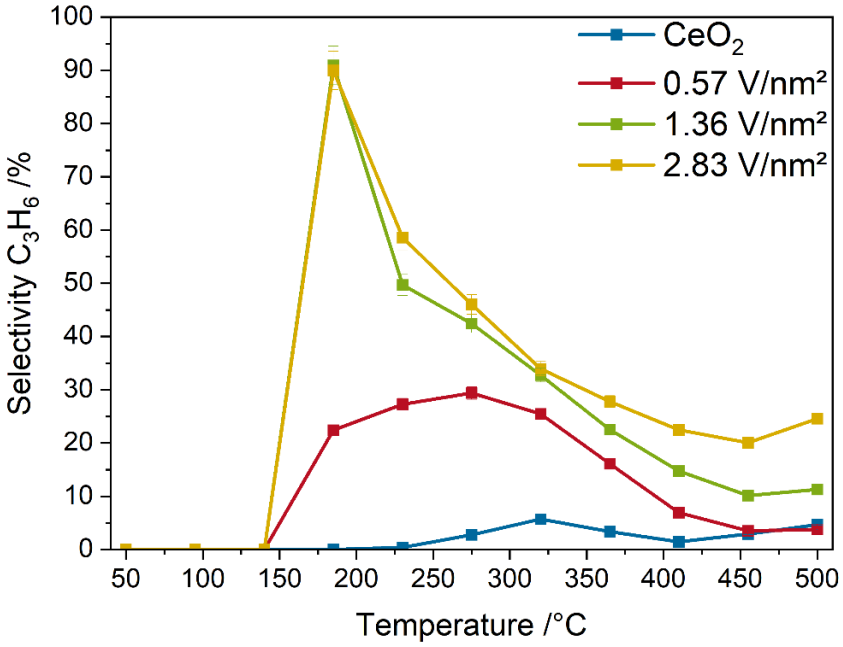

Figure S7: Selectivities of VO_x/CeO_2 catalysts and bare ceria during propane ODH between 50 and 500 °C. Uncertainties are represented by error bars.

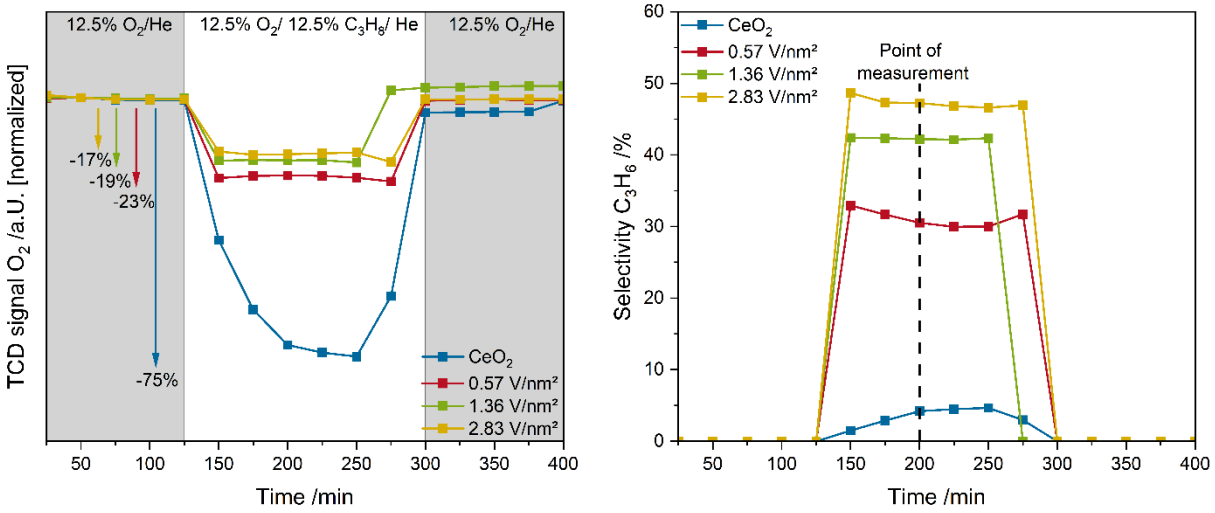

Figure S8: Oxygen TCD signal (left) detected for bare ceria and vanadia-loaded samples in 12.5% O_2/ He and 12.5% O_2/ 12.5% C_3H_8/ He at 275 °C. The decrease in the detected oxygen amount is indicated for each sample. The TCD signal was normalized to eliminate all external effects on the oxygen concentration. The selectivities of the samples (right) measured over the same time frame as the oxygen concentrations.

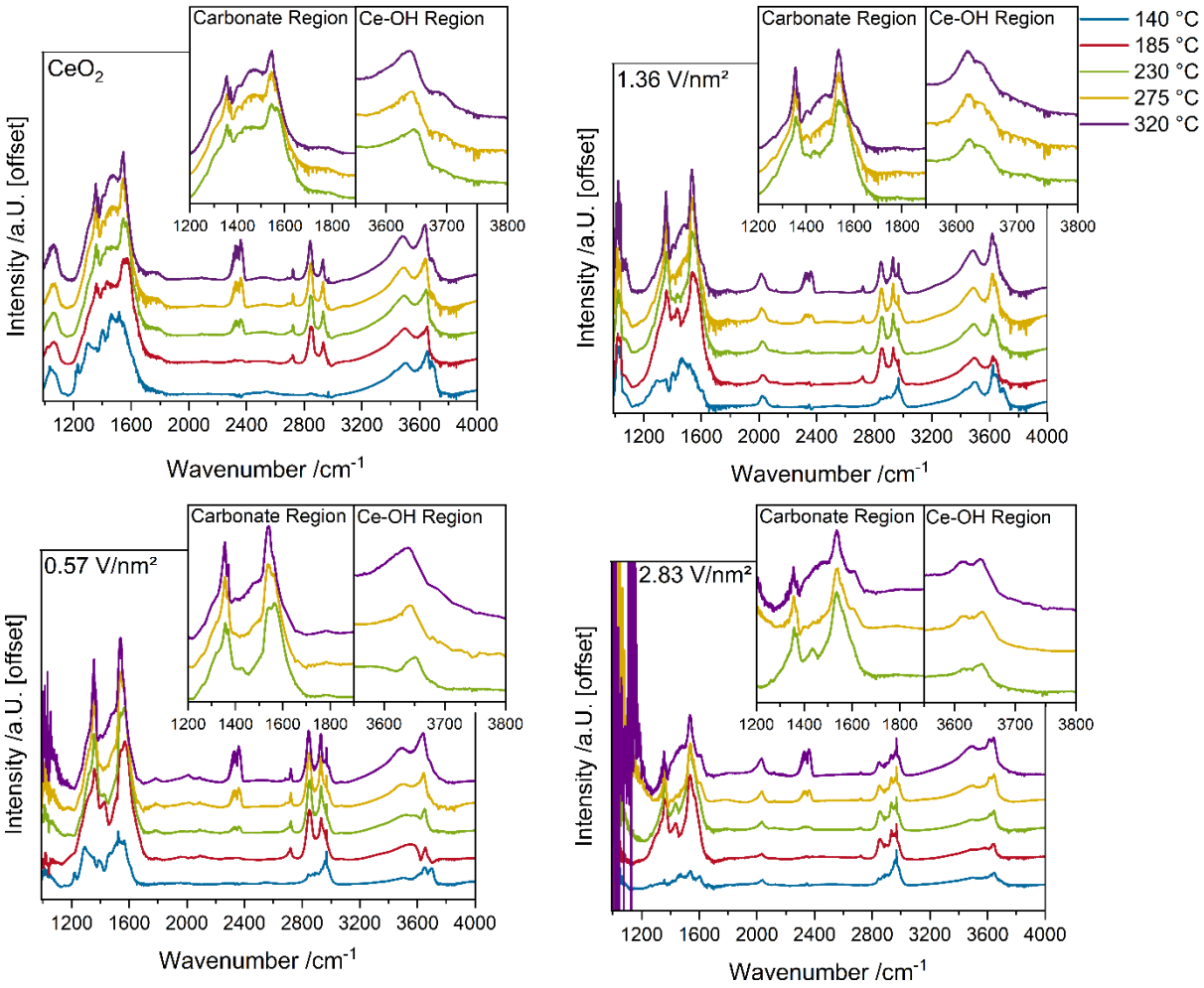

Figure S9: *Operando* DRIFT spectra of VO_x/CeO_2 catalysts and bare ceria upon exposure to 12.5% C_3H_8/ 12.5 % O_2/ He between 140 °C and 320 °C, recorded in 45 °C steps. Spectra at temperatures below 140 °C resemble those at 140 °C.

The spectra in Fig. S9 show significant signals in the carbonate (1200–1900 cm^{-1}), and Ce-OH (3500–3800 cm^{-1}) regions, as indicated by the insets in Fig. S9. Furthermore, at some temperatures, peaks assigned to CO_2 (~2200–2400 cm^{-1}) and adsorbed propane[4,5] (2700–2900 cm^{-1}) can be observed. First, the onset of the reaction is indicated by the appearance of the CO_2 signal, as the total oxidation of propylene occurs as a follow-up reaction to the oxidation to propane at all temperatures. We can therefore conclude that the onset temperature for the reaction is the lowest for ceria and the 0.57 V/nm² sample, where CO_2 is already detected at 230 °C, and then starts to increase with higher vanadia loadings, strongly correlating with the observed conversions. Furthermore, adsorbates detected below the onset temperatures show varying intensity, which depends on the vanadium loading. For example, the intensity

of propane is highest for ceria and decreases with higher loadings, which is consistent with previous results.[6]

At the same temperature, the adsorbates observed in the DRIFT spectra of VO_x/CeO_2 samples largely resemble each other. The most significant differences between samples are observed for the vanadyl stretching mode at ~1010 cm^{-1} and its overtone at ~2025 cm^{-1}. Further differences include additional Ce-OH signals at ~3610 cm^{-1} and 3720 cm^{-1} (only present for the 1.36 and 2.83 V/nm² samples) as well as a signal at 1610 cm^{-1}, which was previously assigned to acrylate adsorbates,[5,7] indicating the possibility of different intermediate states on the catalyst surface at higher loadings. Table S1 summarizes the peak assignments for the spectra recorded at 275 °C.

Table S1: Peak assignments for the DRIFT spectra of the VO_x/CeO_2 samples and bare ceria recorded at 275 °C during reaction conditions (12.5 % C_3H_8/ 12.5 % O_2/ He).

Position /cm^{-1}	Assignment	Reference
1008	V=O	8
1305	υ_s C-O	5
1355	υ_s CH_3	5
1403	δ_s CH_3	5
1471	δ_{as} CH_3	5
1545	υ_{as} COO	5
1567	υ_{as} COO	5
1610	υ_{as} C=C	5
1780	υ C-O	3
2025	V=O overtone	9
2686	υ C-H	6
2722	υ C-H	4
2843	υ CH_2	5
2928	υ CH_2	5
3619	V-O-H	10
3642	Ce-O-H II-B	2
3695	Ce-O-H II-A	2
3740	Ce-O-H I	2

3) *Operando* Spectroscopic Data

a) *Operando* DRIFTS

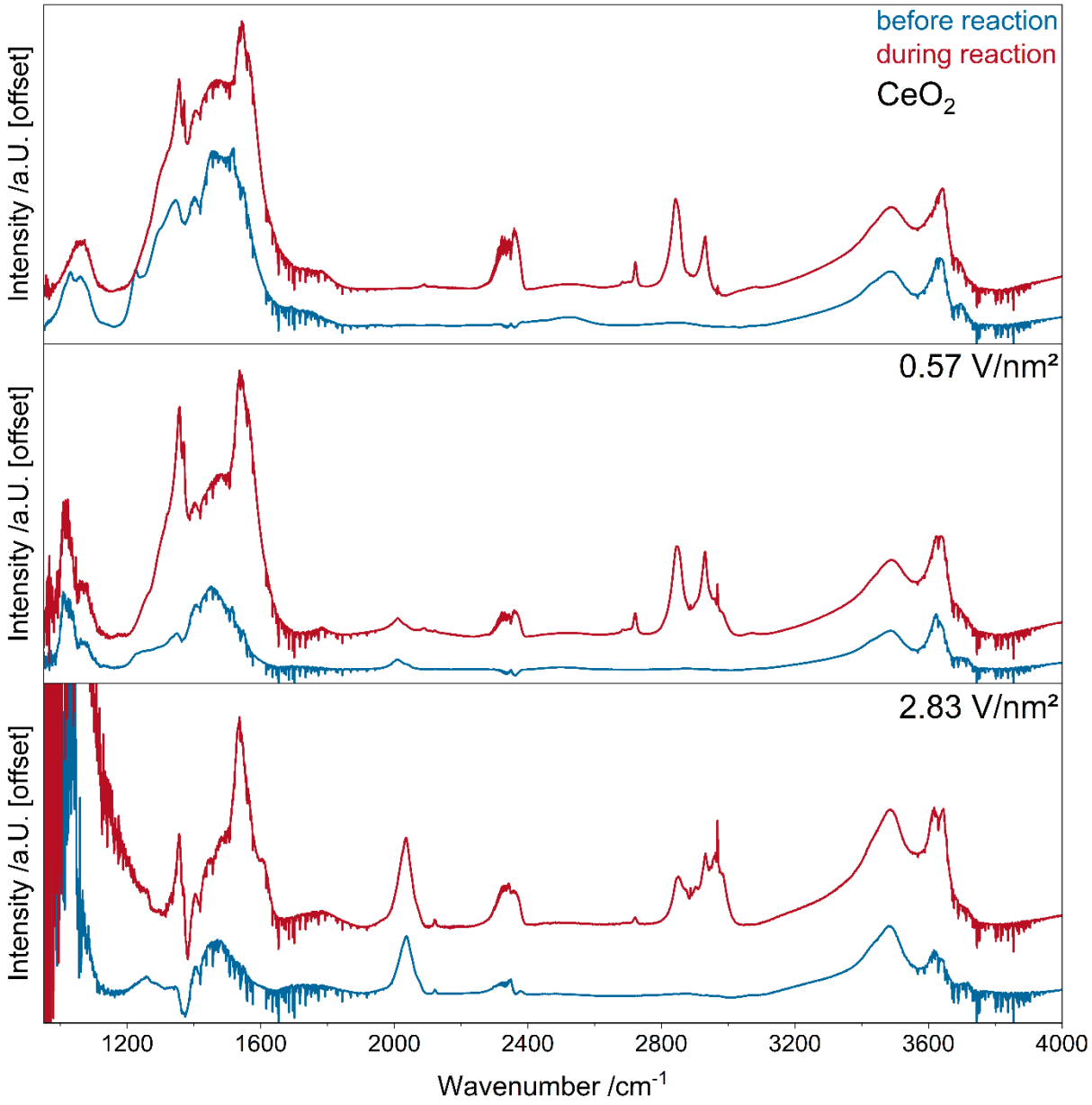

Figure S10: *Operando* DRIFT spectra of ceria, 0.57 V/nm², and 2.83 V/nm² samples. Spectra were recorded at 275 °C under oxidative (blue; 12.5% O_2/He) and reactive (red; 12.5% C_3H_8/12.5% O_2/He) conditions. The spectra are offset for clarity.

b) *Operando* UV-Vis Spectroscopy

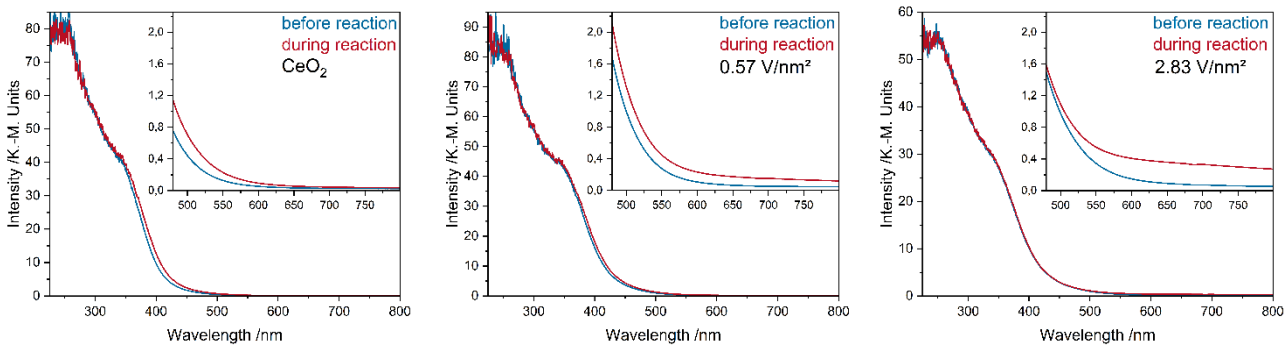

Figure S11: *Operando* UV-Vis spectra of ceria, 0.57 V/nm², and 2.83 V/nm². Spectra were recorded at 275 °C under oxidative (blue; 12.5% O_2/He) and reactive (red; 12.5% C_3H_8/12.5% O_2/He) conditions. For clarity, the insets give an enlarged view of the region 480–800 nm showing the d-d transition region of vanadia.

c) Multi-Wavelength *Operando* Raman Spectroscopy

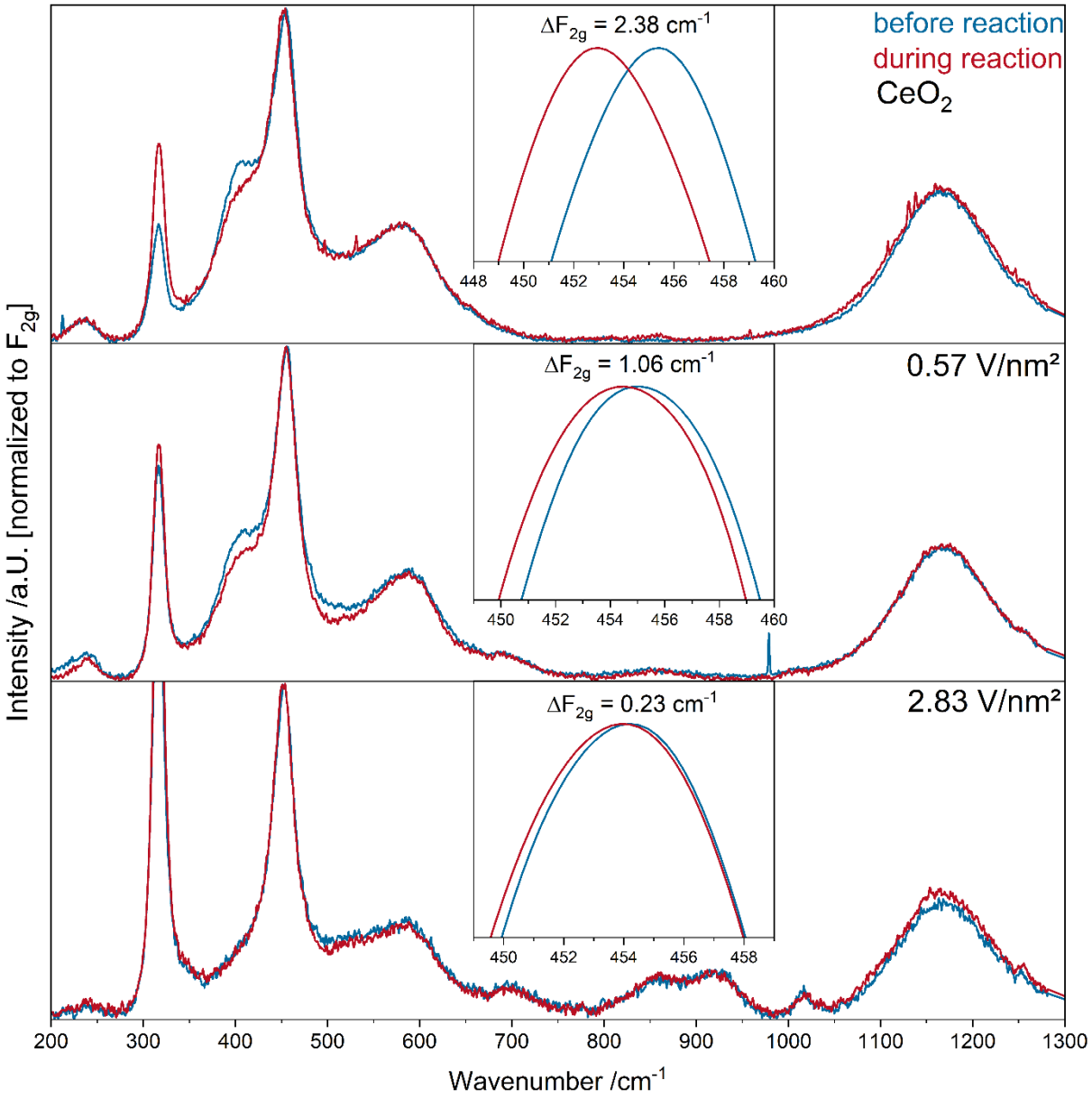

Figure S12: *Operando* UV-Raman spectra (385 nm) of ceria, 0.57 V/nm², and 2.83 V/nm² samples. Spectra were recorded at 275 °C under oxidative (blue; 12.5% O_2/He) and reactive (red; 12.5% C_3H_8/12.5% O_2/He) conditions. The insets show the corresponding ceria F_{2g} modes upon switching from oxidative to reactive conditions, recorded at 532 nm excitation. The red-shifts were determined from a peak-fit analysis.

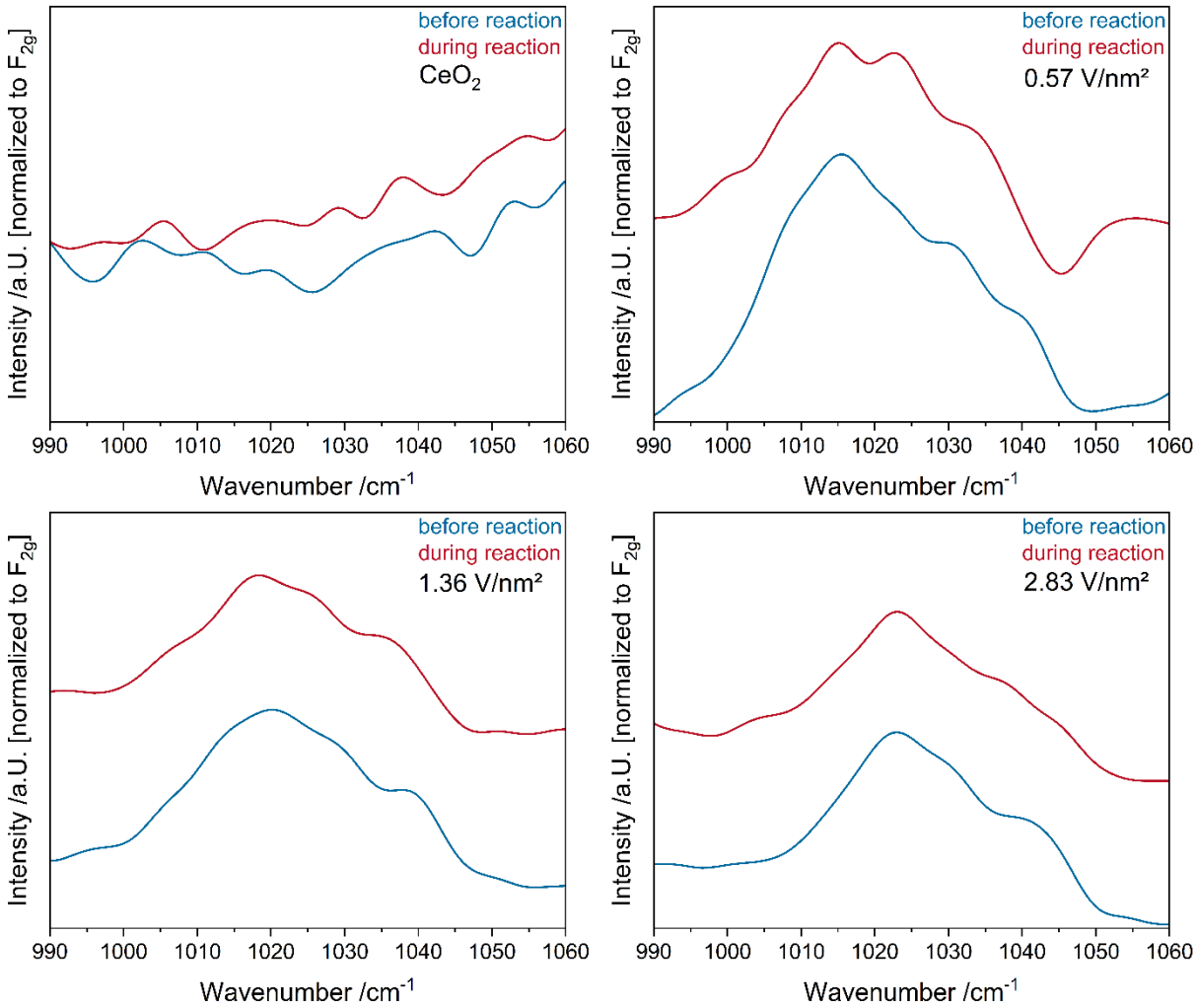

Figure S13: *Operando* Vis-Raman spectra (514 nm) of the vanadyl region of ceria, 0.57 V/nm², 1.36 V/nm², and 2.83 V/nm² samples. Ceria is shown as a reference. Spectra were recorded at 275 °C under oxidative (blue; 12.5% O_2/He) and reactive (red; 12.5% C_3H_8/12.5% O_2/He) conditions.

d) *Operando* Spectroscopic Trends

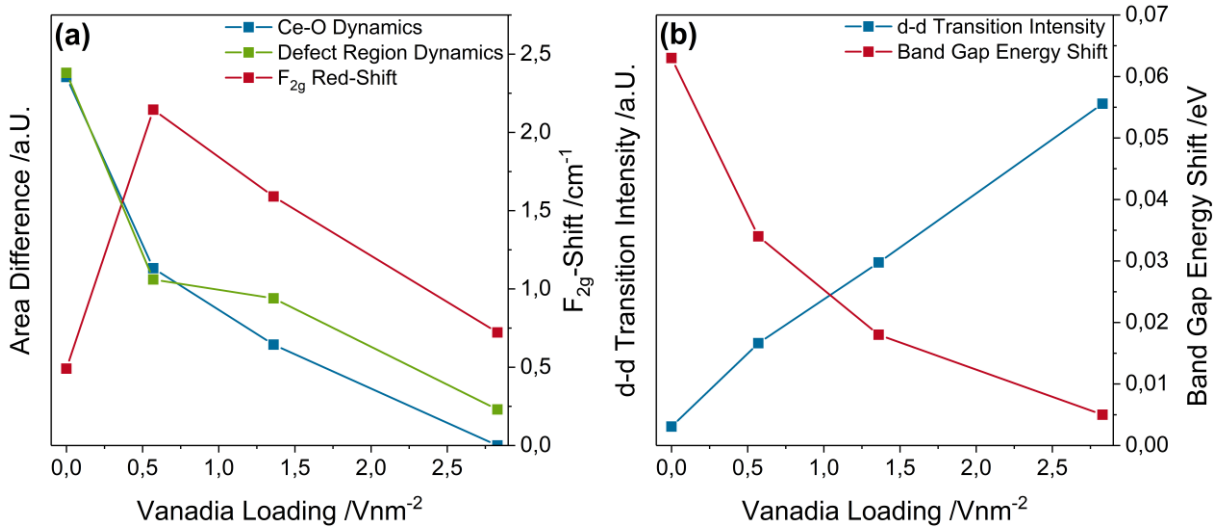

Figure S14: Loading-dependent behavior of the **(a)** Ce-O surface phonon peak, the defect region area, and the F_{2g} position upon exposure to reactive conditions, as determined from 385 and 514 nm Raman spectra. **(b)** d-d transition intensity determined by the difference in UV-Vis absorption intensity at 700 nm and the band-gap shift between oxidative and reactive conditions resulting from Tauc plots.

4) ME-DRIFTS Data

a) MES Principle

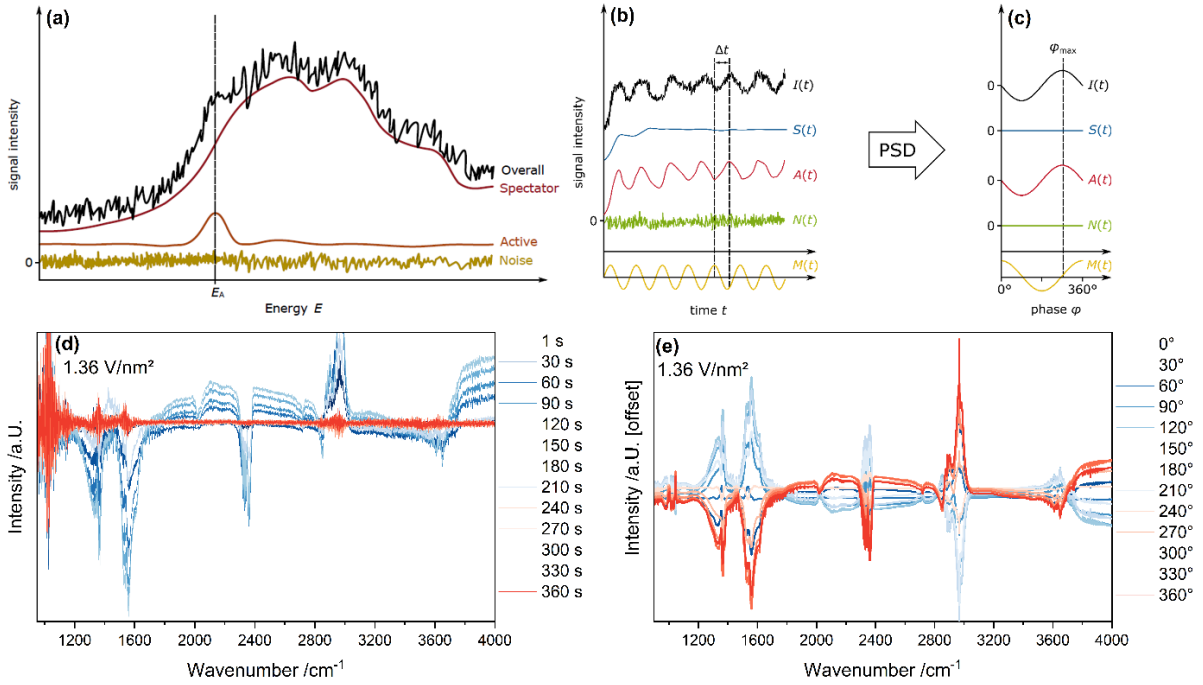

Figure 15: (a) Schematic representation of the contributions to a DRIFTS signal, and **(b)** their response to a concentration modulation M(t). **(c)** Fourier transformation allowing one to extract those contributions oscillating with the modulation and to determine their phase shift. **(d)** Exemplary time-resolved spectra of the 1.36 V/nm² sample, shown after 30 s steps for one period, and **(e)** corresponding Fourier transformed (PSD) spectra with a 30° phase resolution.

Figures S15 a and b show typical contributions (noise, spectator, active species) to a regular DRIFTS signal and their temporal response to a concentration modulation M(t). Importantly, only active species follow the periodic modulation with a characteristic phase shift, which allows their separation via Fourier transformation, resulting in the PSD (phase sensitive detection) spectra shown in Fig. S15c.

To illustrate this process, Figs. S15 d and e show example data for the 1.36 V/nm² sample for constant propane flow and modulated oxygen flow. For the time-resolved data (see d), spectra are shown every 30 s. Note that the background subtracted from each spectrum was measured in 12.5% O_2/He so that only changes during propane exposure are observed. Figure S15 e depicts the corresponding PSD spectra every 30° (see Figs. S16 and S17 for the other samples), adjusted for spectator species and with significantly improved background and noise reduction in comparison to Fig. 2c.

b) PSD Spectra in Different Gas Atmospheres

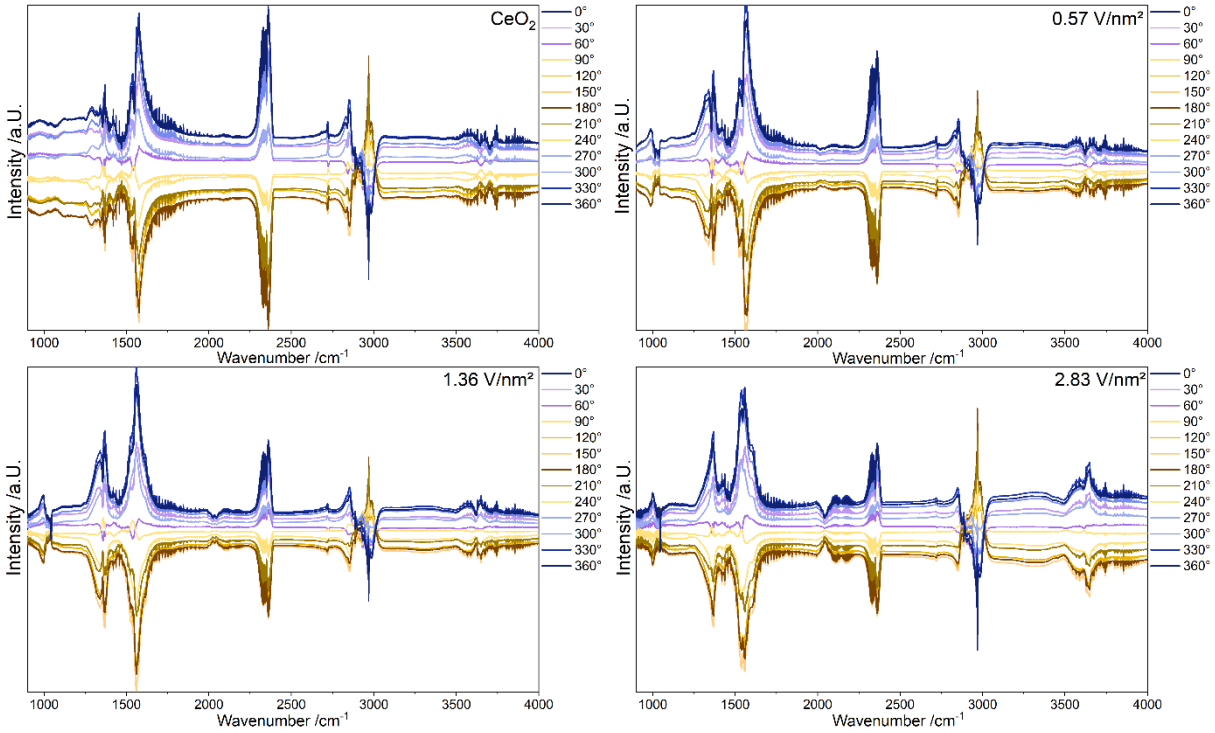

Figure S16: PSD spectra of VO_x/CeO_2 samples and bare ceria recorded at 275 °C under constant oxygen flow and pulsed propane flow with 30° phase resolution.

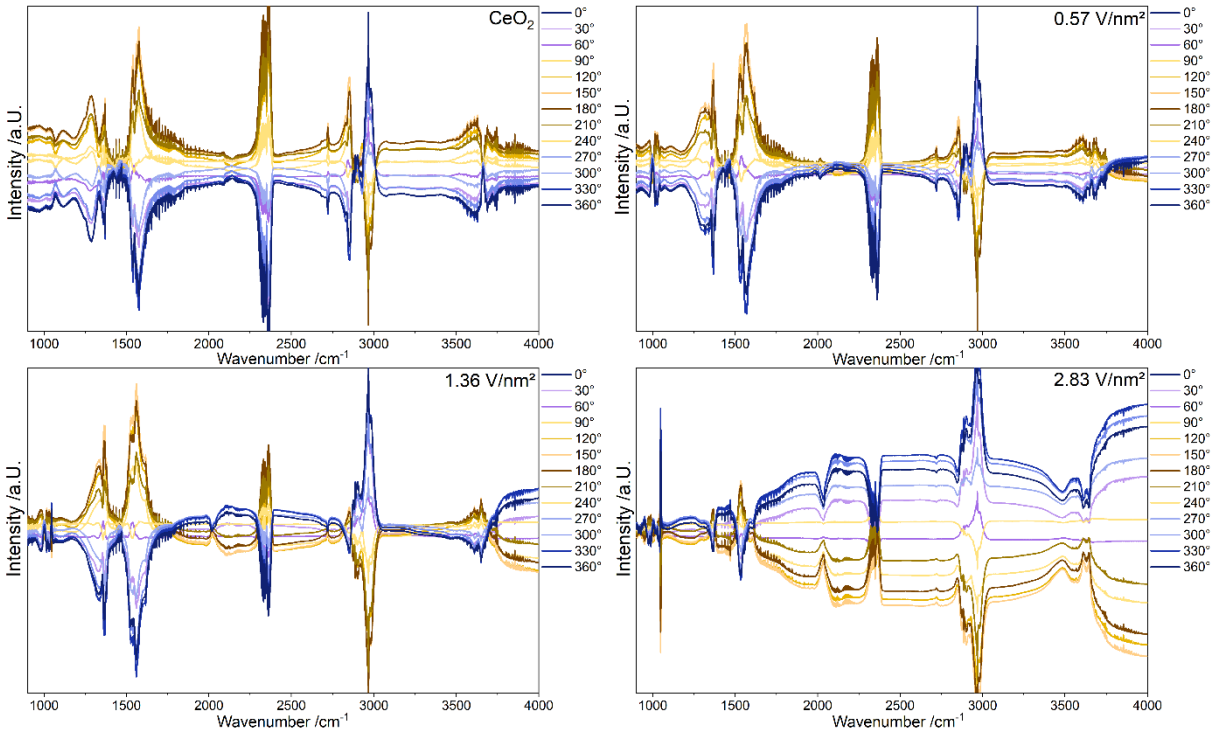

Figure S17: PSD spectra of VO_x/CeO_2 samples and bare ceria recorded at 275 °C under constant propane flow and pulsed oxygen flow with a 30° phase resolution.

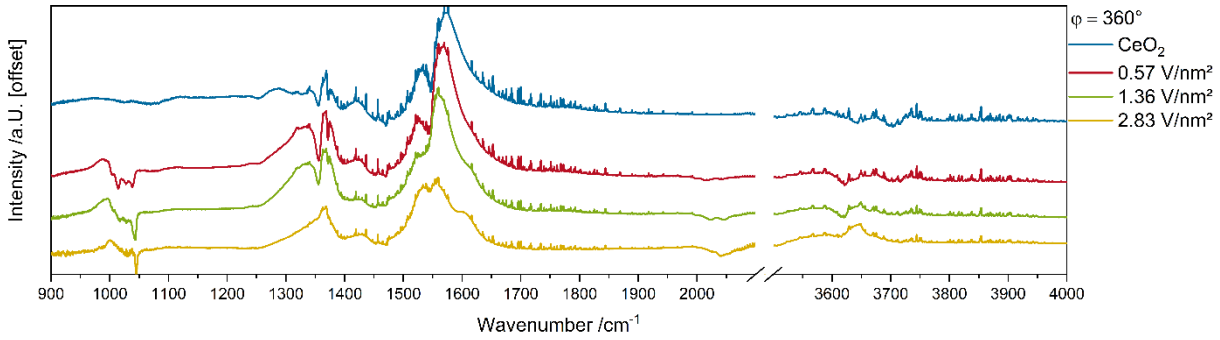

Figure S18: PSD spectra of VO_x/CeO_2 samples and bare ceria recorded at 275 °C in a constant oxygen and a pulsed propane flow at a phase-shift of 360°. For clarity, the region 2100–3500 cm^{-1}, in which only gas-phase-related features (CO, CO_2, and C_3H_8) were observed, has been cut out.

When comparing the two modulated gas-phase compositions in Figs. 3a and S18, significant differences between the carbonate regions, especially for bare ceria and the sample loaded with 2.83 V/nm², as well as the OH region become apparent. This difference can be explained by the fact that the observer species are most likely not completely eliminated during the constant oxygen and modulated propane gas phase. When oxygen and propane are flowing simultaneously over the sample, all adsorbates present during the reaction as well as observer species are created. When the propane is subsequently removed, the O_2/He flow is likely to completely regenerate the catalyst surface, resulting in an intensity change of all adsorbed species, including observer species. In contrast, when propane flows constantly and oxygen is modulated, only adsorbate species relevant for propane ODH are expected to be observed. During the C_3H_8/He gas phase, all adsorbed species, including observer species, are created. When oxygen is subsequently pulsed onto the catalyst, it enables the ODH reaction with the adsorbates relevant for the reaction, resulting in an intensity change of these species only.

When comparing all PSD spectra using a 30° phase resolution (compare Figs. S16 and S17), a broad background starting between 1500 and 2000 cm^{-1} up to 4000 cm^{-1} is observed, which increases towards higher wavenumbers. The background during constant oxygen and pulsed propane flow has a comparably small intensity and does not differ between ceria- and vanadia-loaded samples. In comparison, the intensity of the background observed for the samples during constant propane and pulsed oxygen

flow is small at low wavenumbers and increases towards higher wavenumbers. Generally, higher vanadium loadings lead to an increased background intensity, which represents a very significant contribution for the 2.83 V/nm² sample. The background may be caused by a reduction of the ceria support[11] or the active vanadium center resulting from the reducing gas atmosphere during the C_3H_8/He exposure. These reduction processes may create electronic states in the band gap that can be excited by IR radiation, as previously observed for supported palladium clusters.[12] Since the background intensity increases towards higher vanadium loadings, it is more likely to be caused by vanadium reduction.

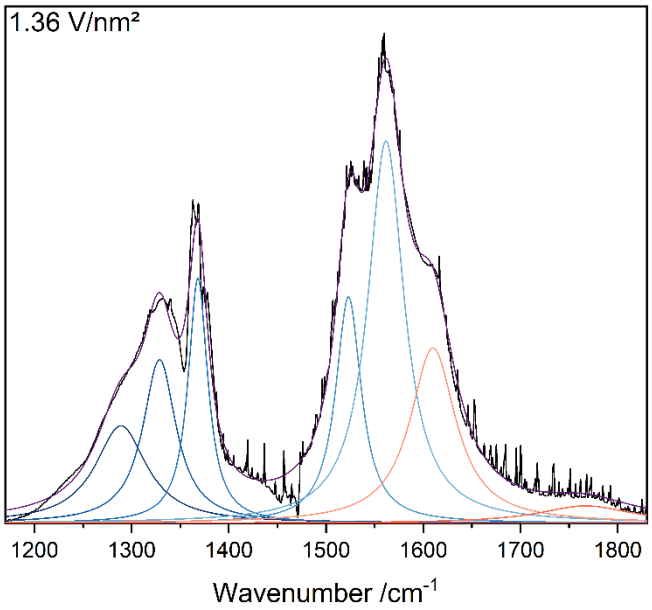

Figure S19: Example fit to the PSD spectrum of the 1.36 V/nm² sample, recorded at 275 °C in constant propane and pulsed oxygen flow at a phase shift of 180°.

c) PSD Spectra During Propane-h8/d8 Modulation

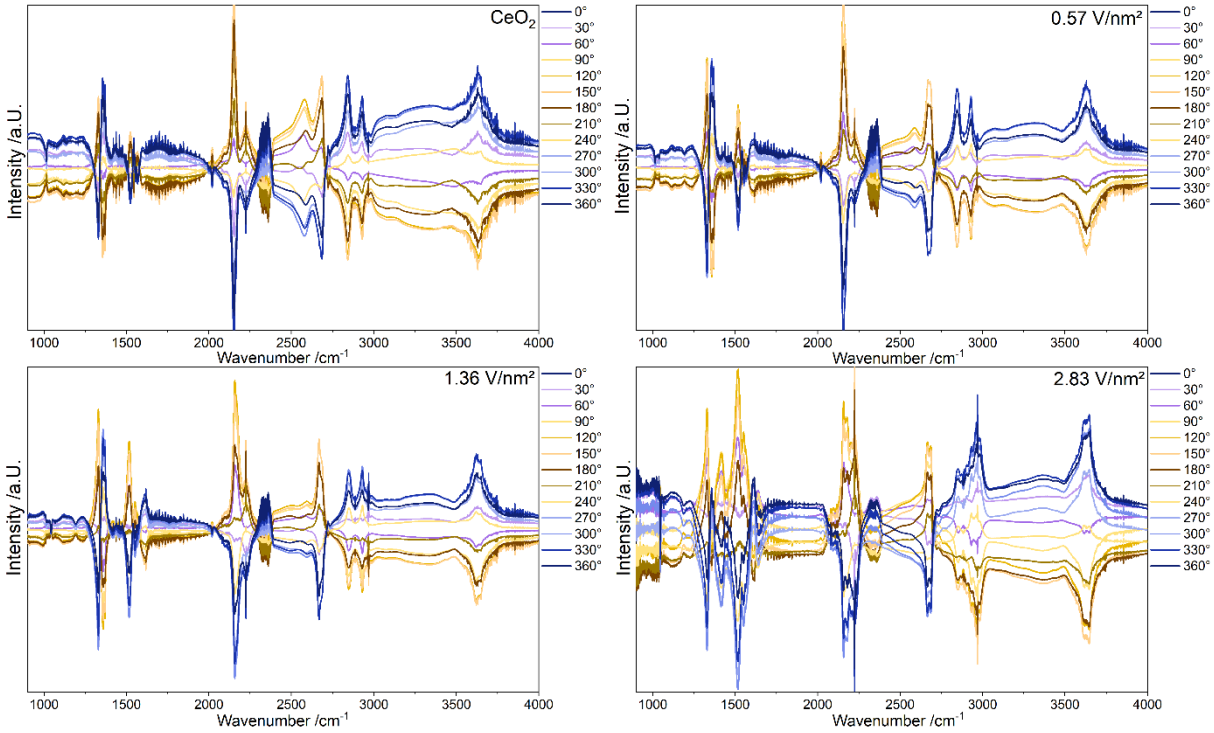

Figure S20: PSD spectra of VO_x/CeO_2 samples and bare ceria recorded at 275 °C under constant oxygen flow and pulsed propane-h8/d8 flow with a 30° phase resolution.

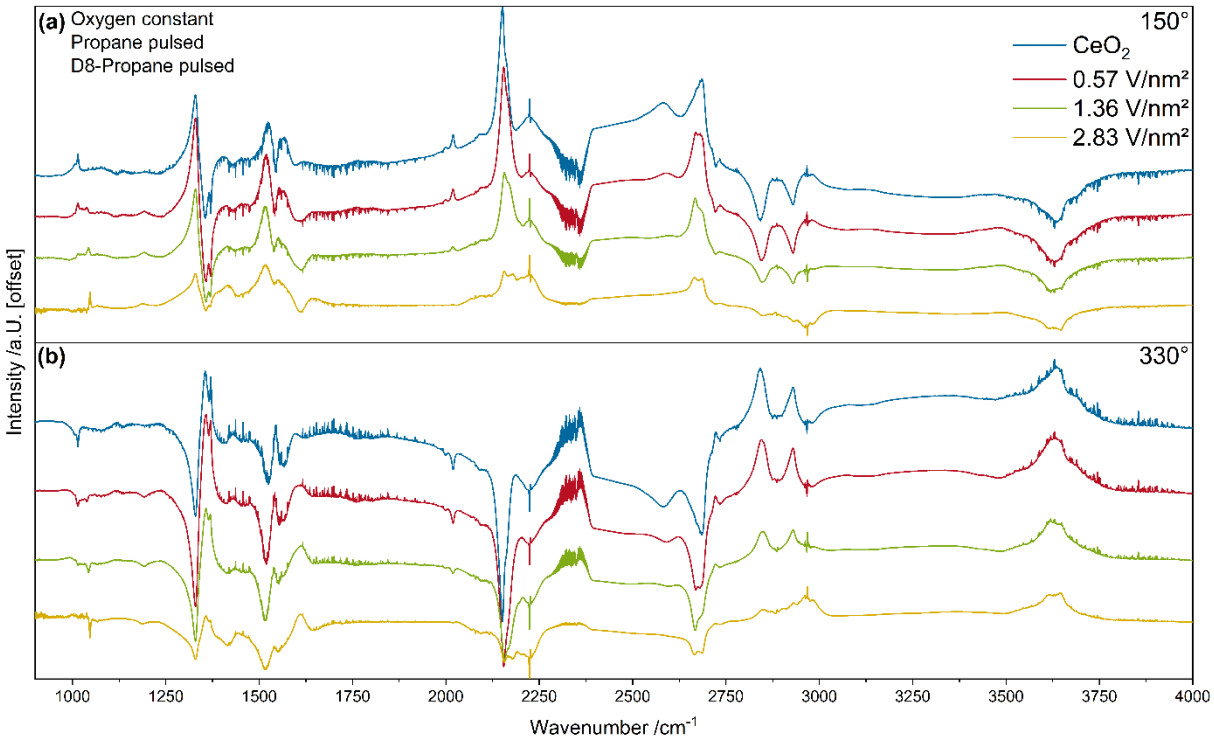

Figure S21: PSD spectra of VO_x/CeO_2 samples and bare ceria recorded at 275 °C under constant oxygen and modulated h8/d8-propane flow. The spectra at phase shifts of 150° **(a)** and 330° **(b)** represent the spectra with the highest peak intensities.

For further insight into the dynamics, we performed isotopic exchange experiments using a constant oxygen flow and a pulsed propane flow that was constantly switched between propane-h8 and propane-d8 (see Fig. S2). This experiment allows peaks to be identified that are associated with a hydrogen transfer during the reaction mechanism, as the only way of introducing hydrogen/deuterium is through propane.

Figures S21 a and b show PSD spectra from the same gas phase but phase-shifted by 180°, representing the spectra with the highest peak intensities (see Fig. S20 for all spectra). The two spectra appear to be mirror images, confirming the validity of the experiment as well as the reversibility of the hydrogen transfer process. There are significant differences between Figs. 3a and S21, in particular in the carbonate region, as the previously intense features below 1300 and above 1500 cm^{-1} are either not observable or drastically reduced in intensity in Fig. 3a, as only hydrogen-containing modes are probed. Similarly, hydrogen-free gas-phase modes are eliminated (see Figs. 3a, S16, S17, S20). Furthermore, the H/D exchange isolates peaks, since for example the Ce-OH peaks above 3500 cm^{-1} appear as Ce-OD signals with similar lineshapes but negative intensities within 2500–2700 cm^{-1}. Small intensities or

changes in the lineshape of peaks that do not contain hydrogen might be caused by the kinetic isotope effect, as the different barriers for C-D and C-H dissociation[13] lead to different reaction rates, resulting in small intensity fluctuations, which are traceable after Fourier transformation. Besides, a new peak appears at ~2150 cm^{-1}, which originates from a CHD vibration and is caused by isotopic scrambling of propane-h8/d8, as described previously.[14]

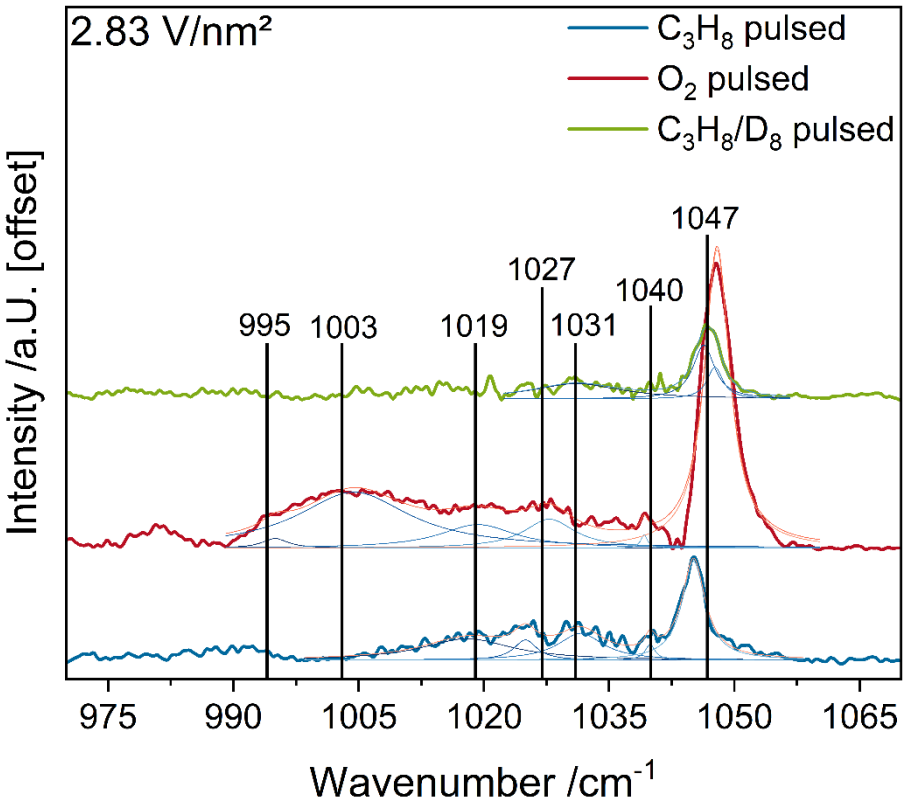

Figure S22: Enlarged view of the vanadyl region of the 2.83 V/nm² sample during different MES experiments at 275 °C, together with the results of a peak fit analysis.

d) In-Phase Angle Analysis and Adsorbate Time Constants

Table S2: Time constants determined from the in-phase angle analysis of bare ceria, 0.57 V/nm², and 2.83 V/nm² samples.

Wavenumber /cm^{-1} CeO_2	**Time /s**	**Wavenumber /cm^{-1} 0.57 V/nm²**	**Time /s**	**Wavenumber /cm^{-1} 2.83 V/nm²**	**Time /s**
1119	14.6	1118	16.7	2017	22.9
3690	15.6	1994	18.7	1331	23.9
1442	16.6	1237.1	19.8	1605	23.9
3735	16.6	1442.9	19.8	1771	23.9
1236	17.7	2017	19.8	1994	23.9
1796	19.8	2037	19.8	2087	23.9
1287	20.8	3686	19.8	3739	23.9
1573	23.9	3734.1	19.8	1436	25
1370	30.2	3611.9	20.8	1567	25
1538	32.3	2087	21.9	2037	25
		1289	22.9	1368	28.1
		1779	22.9	3644	28.1
		1615	23.9	3611.9	29.1
		1378	25	1533	30.2
		1333	26		
		1566	27.1		
		3648	30.2		
		1368	32.3		
		1530	33.3		

Table S3: Time constants determined (three times) from the in-phase angle analysis of the 1.36 V/nm² sample that were used for the determination of the error bars shown in Table 2.

Wavenumber /cm^{-1} 1.36 V/nm² (1)	Time /s	Wavenumber /cm^{-1} 1.36 V/nm² (2)	Time /s	Wavenumber /cm^{-1} 1.36 V/nm² (3)	Time /s
1994	17.7	1994	21.8	1994	18.7
2017	18.7	2017	22.8	2017	18.7
3608	18.7	3608	20.8	3608	18.7
3730	18.7	3730	21.8	3730	18.7
2037	18.7	2037	22.8	2037	19.7
1441	19.7	1441	22.8	1441	20.8
1768	20.8	1768	23.9	1768	20.8
2087	19.7	2087	23.9	2087	20.8
1289	22.8	1289	24.9	1289	23.9
1608	24.9	1608	27	1608	26
3650	23.9	3650	27	3650	23.9
1329	27	1329	29.1	1329	28
1561	31.2	1561	32.2	1561	32.2
1523	32.2	1523	32.2	1523	32.2
1368	33.2	1368	35.3	1368	34.3

References

(1) Ji, Y.; Toops, T. J.; Graham, U. M.; Jacobs, G.; Crocker, M. A Kinetic and DRIFTS Study of Supported Pt Catalysts for NO Oxidation. *Catal. Lett.* **2006**, *110* (1-2), 29–37. DOI: 10.1007/s10562-006-0100-4.

(2) Badri, A.; Binet, C.; Lavalley, J.-C. An FTIR Study of Surface Ceria Hydroxy Groups During a Redox Process With H_2. *Faraday Trans.* **1996**, *92* (23), 4669. DOI: 10.1039/ft9969204669.

(3) Li, C.; Sakata, Y.; Arai, T.; Domen, K.; Maruya, K.-i.; Onishi, T. Carbon Monoxide and Carbon Dioxide Adsorption on Cerium Oxide Studied by Fourier-Transform Infrared Spectroscopy. Part 1. – Formation of Carbonate Species on Dehydroxylated CeO_2 at Room Temperature. *J. Chem. Soc., Faraday Trans. 1* **1989**, *85* (4), 929. DOI: 10.1039/f19898500929.

(4) Hu, Z.; Liu, X.; Meng, D.; Guo, Y.; Guo, Y.; Lu, G. Effect of Ceria Crystal Plane on the Physicochemical and Catalytic Properties of Pd/Ceria for CO and Propane Oxidation. *ACS Catal.* **2016**, *6* (4), 2265–2279. DOI: 10.1021/acscatal.5b02617.

(5) Hu, Z.; Wang, Z.; Guo, Y.; Wang, L.; Guo, Y.; Zhang, J.; Zhan, W. Total Oxidation of Propane over a Ru/CeO_2 Catalyst at Low Temperature. *Environ. Sci. Technol.* **2018**, *52* (16), 9531–9541. DOI: 10.1021/acs.est.8b03448.

(6) Schumacher, L.; Hess, C. The Active Role of the Support in Propane ODH over VO_x/CeO_2 Catalysts Studied Using Multiple Operando Spectroscopies. *J. Catal.* **2021**, *398* (13), 29–43. DOI: 10.1016/j.jcat.2021.04.006.

(7) Novakova, E.; Vedrine, J.; Derouane, E. Propane Oxidation on Mo–V–Sb–Nb Mixed Oxide Catalysts. Influence of Catalyst Activation Methods on the Reaction Mechanism. *J. Catal.* **2002**, *211* (1), 235–243. DOI: 10.1016/s0021-9517(02)93705-x.

(8) Baron, M.; Abbott, H.; Bondarchuk, O.; Stacchiola, D.; Uhl, A.; Shaikhutdinov, S.; Freund, H.-J.; Popa, C.; Ganduglia-Pirovano, M. V.; Sauer, J. Resolving the Atomic Structure of Vanadia Monolayer Catalysts: Monomers, Trimers, and Oligomers on Ceria. *Angew. Chem. Int. Ed.* **2009**, *121* (43), 8150–8153. DOI: 10.1002/ange.200903085.

(9) Burcham, L. J.; Deo, G.; Gao, X.; Wachs, I. E. In-Situ IR, Raman, and UV-Vis DRS Spectroscopy of Supported Vanadium Oxide Catalysts During Methanol Oxidation. *Top. Catal.* **2000**, *11/12* (1/4), 85–100. DOI: 10.1023/A:1027275225668.

(10) Sambeth, J. E.; Centeno, M. A.; Paúl, A.; Briand, L. E.; Thomas, H. J.; Odriozola, J. A. In Situ DRIFTS Study of the Adsorption-Oxidation of CH_3OH on V_2O_5. *J. Mol. Catal. A: Chem.* **2000**, *161* (1-2), 89–97. DOI: 10.1016/S1381-1169(00)00152-7.

(11) Panayotov, D. A.; Burrows, S. P.; Morris, J. R. Infrared Spectroscopic Studies of Conduction Band and Trapped Electrons in UV-Photoexcited, H-Atom n-Doped, and Thermally Reduced TiO_2. *J. Phys. Chem. C* **2012**, *116* (7), 4535–4544. DOI: 10.1021/jp2053103.

(12) Chiarello, G. L.; Lu, Y.; Agote-Arán, M.; Pellegrini, R.; Ferri, D. Changes of Pd Oxidation State in Pd/Al_2O_3 Catalysts Using Modulated Excitation DRIFTS. *Catalysts* **2021**, *11* (1), 116. DOI: 10.3390/catal11010116.

(13) Ni, Y.; Ma, Q.; Ellis, G. S.; Dai, J.; Katz, B.; Zhang, S.; Tang, Y. Fundamental Studies on Kinetic Isotope Effect (KIE) of Hydrogen Isotope Fractionation in Natural Gas Systems. *Geochim. Cosmochim. Acta* **2011**, *75* (10), 2696–2707. DOI: 10.1016/j.gca.2011.02.016.

(14) Friedman, L.; Turkevich, J. The Infra-Red Absorption Spectra of Propane-D-1 and Propane-D-2. *J. Chem. Phys.* **1949**, *17* (11), 1012–1015. DOI: 10.1063/1.1747105.